

# Model Development and Validation of Samarium Doped Ceria (SDC) Based Solid Oxide Fuel Cell Operating with Practical Fuels



by

Mazni Ismail

A thesis  
presented to the University of Waterloo  
in fulfillment of the  
thesis requirement for the degree of  
Doctor of Philosophy  
in  
Chemical Engineering

Waterloo, Ontario, Canada, 2013

© Mazni Ismail 2013



## Abstract

Solid Oxide Fuel Cell (SOFC) is a promising technology for producing electricity cleanly and efficiently. This type of fuel cell is a high temperature fuel cell operating around 1000°C for state-of-the-art SOFC. An advantage of the high temperature is the possibility of combined heat and power generation which would even further increase the efficiency of this technology. However, due to high operating temperatures, there are problems associated with the development and commercialization of SOFC, such as requirement of high temperature gas seals, and relatively poor long-term stability. The current trend in SOFC development is therefore to reduce the operating temperature of the cell to the range 600-800°C. However, this requires developing new cell designs and materials since decreasing the operating temperature increases the ohmic overpotential due to higher ionic diffusion resistance in the electrolyte, thereby reducing electrochemical performance. For intermediate temperature SOFC, SDC is a promising electrolyte material to reduce the ohmic overpotential.

The present research focused on developing a 1D model of SDC based SOFC validated for a number of feed gas compositions, from humidified  $H_2$ , mixture of CO and  $CO_2$ , to several syngas compositions (typical of diesel syngas, biomass syngas and pre-reformed natural gas). The model was developed for an anode supported cell. Few parameters were used as free fit parameters: essentially structural parameters, such as porosity and tortuosity, as well as kinetic parameters for  $H_2$  and CO electrochemical reactions. In most cases, the simulated results (polarization curve) fitted well the experimental data. It was seen that the performance of CO/ $CO_2$  system is considerably lower than the  $H_2/H_2O$  system. The model results also allowed to access variables' profiles that would not be accessible experimentally, such species composition profile and local current density along the anode. In particular, it was observed that most the electrochemical reaction occurred within 10  $\mu m$  away from the anode/electrolyte interface.

In the literature, the water-gas shift (WGS) reaction is considered to occur only over Ni, but the present work demonstrated that SDC is active toward the WGS reaction. Therefore, a kinetic study was carried out to determine a rate expression for the WGS reaction. This rate

expression was then incorporated into the SOFC model. The results indicated that inclusion of the WGS reaction on SDC has minor or negligible effect in most situations, except in the case of CO mole fraction for the diesel syngas feed at higher cell voltage. The reason was that the composition of diesel syngas was such that there was a higher driving force for the WGS reaction to proceed in the reverse WGS direction. When the water content is high enough, as in the case of higher current densities, the form of the derived rate expression for the WGS on SDC makes the value of this rate very small. The rate expression was derived using relatively small amounts of water because of experimental limitation and therefore, the form of this rate needs to be revisited by considering higher amount of water.

## Table of Contents

AUTHOR'S DECLARATION .....	ii
Abstract .....	iii
Acknowledgements .....	v
Dedication .....	vi
Table of Contents .....	vii
List of Figures .....	ix
List of Tables.....	xii
Nomenclature .....	xiii
Chapter 1 Introduction.....	1
1.1 Motivation of the Research .....	3
1.2 Research Contributions .....	4
1.3 Thesis Outline.....	4
Chapter 2 Literature Review .....	6
2.1 Introduction .....	6
2.2 Fuel Cells in Brief .....	6
2.3 Solid Oxide Fuel Cell .....	10
2.4 Summary of SOFC Modelling Studies.....	23
Chapter 3 Experimental - Apparatus and Procedures.....	35
3.1 Material Preparation .....	35
3.1.1 Material Preparation for Methane Steam Reforming (MSR) Experimental Work.....	35
3.1.2 Material Preparation for Reverse Water Gas Shift (RWGS) Reaction Experimental Work	36
3.2 Fixed Bed Reactor for Catalyst Performance Experiments.....	36
3.3 SOFC Button cell Electrochemical Performance Measurement .....	42
Chapter 4 Kinetic Study of Reverse Water Gas Shift Reaction .....	49
4.1 Introduction .....	49
4.2 Methane Steam reforming on YSZ/Ni-YSZ and SDC/Ni-SDC .....	49
4.3 Reverse Water Gas Shift Reaction on SDC and YSZ .....	55
4.4 Kinetics of reverse Water Gas Shift Reaction on SDC .....	59
4.5 Markov Chain Monte Carlo Study .....	76
Chapter 5 Model Formulation .....	86
5.1 Introduction .....	86



5.2 Mass Transport in Anode and Cathode.....	89
5.2.1 Reaction Rate Calculation.....	92
5.3 Charge Transport .....	95
Chapter 6 SOFC Modelling, Calibration and Validation.....	99
6.1 H <sub>2</sub> /H <sub>2</sub> O Model Validation and Discussion.....	100
6.2 CO/CO <sub>2</sub> Model Validation and Discussion.....	105
6.3 Comparison between H <sub>2</sub> and CO Electrochemical Oxidation .....	109
6.4 Syngas Model Validation and Discussion .....	110
Chapter 7 Conclusions and Recommendations.....	121
7.1 Conclusions.....	121
7.2 Recommendations.....	125
Appendix A Matlab Codes.....	127
Appendix B Derivation of rs1 rate expression .....	134
Appendix C Arrhenius Plots for Each Limiting Steps.....	137
Bibliography .....	146

## List of Figures

Figure 2.1: Diagram of a single fuel cell (Lisbona et al., 2005).....	7
Figure 2.2: Schematic diagram of SOFC operation .....	11
Figure 2.3: SOFC design (Singhal, 2000; Yamamoto, 2000) .....	19
Figure 2.4: Ideal performance of fuel cells.....	21
Figure 2.5: Actual performance of fuel cells.....	22
Figure 3.1: Procedure for preparing NiO powder.....	36
Figure 3.2: Catalysis activity test station.....	37
Figure 3.3: Quartz tube reactor.....	39
Figure 3.4: a) Electrolyte-anode bilayer; b) NiO/SDC anode-supported cell .....	43
Figure 3.5: A schematic diagram of SOFC test station .....	45
Figure 3.6: SOFC cell set-up.....	47
Figure 4.1: Methane conversion for SDC and YSZ at 750 and 650°C (S/C = 3, GHSV ~ 140 h <sup>-1</sup> ).....	50
Figure 4.2: Methane conversion for Ni-SDC and Ni-YSZ catalysts at different temperatures (S/C = 3, GHSV ~ 140 h <sup>-1</sup> ).....	52
Figure 4.3: H <sub>2</sub> yield for Ni-YSZ and Ni-SDC at different temperatures (S/C=3; GHSV~ 140 h <sup>-1</sup> ).....	54
Figure 4.4: CO yield for Ni-YSZ and Ni-SDC at different temperatures (S/C= 3; GHSV~140 h <sup>-1</sup> ) ...	54
Figure 4.5: CO <sub>2</sub> conversion for reverse WGS reaction over SDC and YSZ at different temperatures (H <sub>2</sub> /CO <sub>2</sub> = 1, GHSV ~ 70 h <sup>-1</sup> ).....	56
Figure 4.6: CO <sub>2</sub> conversion for reverse WGS reaction over SDC and YSZ at different temperatures (H <sub>2</sub> /CO <sub>2</sub> = 3, GHSV ~ 70 h <sup>-1</sup> ).....	56
Figure 4.7: CO <sub>2</sub> conversion for reverse WGS reaction over SDC and YSZ at different temperatures (H <sub>2</sub> /CO <sub>2</sub> = 4, GHSV ~ 70 h <sup>-1</sup> ).....	57
Figure 4.8: CO <sub>2</sub> conversion for reverse WGS reaction over SDC at different temperatures and H <sub>2</sub> /CO <sub>2</sub> ratios (GHSV ~ 70 h <sup>-1</sup> ) .....	58
Figure 4.9: CO <sub>2</sub> conversion for reverse WGS reaction over YSZ at different temperatures and H <sub>2</sub> /CO <sub>2</sub> ratios (GHSV ~ 70 h <sup>-1</sup> ) .....	58
Figure 4.10: Reaction rate versus flow rate for different particle diameters at two different temperatures (CO <sub>2</sub> /H <sub>2</sub> =1, GHSV=640h <sup>-1</sup> ) .....	60
Figure 4.11: Comparison of CO <sub>2</sub> conversion to the equilibrium conversion at two different temperatures for particle size of 210 micrometer and flow rate of 280 ml/min (CO <sub>2</sub> /H <sub>2</sub> =1, GHSV=640h <sup>-1</sup> ) .....	61

Figure 4.12: Comparison between experiments and simulation for the conversion of CO <sub>2</sub> at 800°C .	70
Figure 4.13: Comparison between experiments and simulation for the conversion of CO <sub>2</sub> at 750°C .	71
Figure 4.14: Comparison between experiments and simulation for the conversion of CO <sub>2</sub> at 700°C .	71
Figure 4.15: Comparison between experiments and simulation for the conversion of CO <sub>2</sub> at 650°C .	72
Figure 4.16: Arrhenius plot of k.....	73
Figure 4.17: Arrhenius plot of K <sub>s</sub> .....	73
Figure 4.18: Arrhenius plot of K <sub>H2O</sub> .....	74
Figure 4.19: Comparison between experiments and simulations for the conversion of CO <sub>2</sub> at temperature of 800-650°C .....	75
Figure 4.20: The gradient plots for parameters k, K <sub>s2</sub> , K <sub>CO</sub> , K <sub>CO2</sub> and K <sub>H2O</sub> as a function of the catalyst weight using data points at 1023 K.....	79
Figure 4.21: The gradient plots for parameters K <sub>CO</sub> and K <sub>CO2</sub> as a function of the catalyst weight using data points at 1073 K .....	80
Figure 4.22: MCMC output values for parameters k, Ks and KH2O at a temperature of 1073 K .....	81
Figure 4.23: A 95% joint confidence region for parameters k and KL and Ek and EKL (below).....	82
Figure 4.24: A plot of predicted values compared with experimentally observed values .....	83
Figure 4.25: Residual plot that measures the difference between the observed and the predicted values .....	83
Figure 5.1: Electron conductivity of SSC (Hui et al., 2010).....	97
Figure 6.1: Experimental (dotted lines) and simulated (solid lines) cell performance using 3% humidified H <sub>2</sub> as fuel source at 700, 650 and 600°C .....	101
Figure 6.2: H <sub>2</sub> and H <sub>2</sub> O molar fractions at 700°C for two different cell voltages (0.7 and 0.5V) .....	102
Figure 6.3: O <sub>2</sub> molar fractions at 700°C for two different cell voltages (0.7 and 0.5V).....	102
Figure 6.4: H <sub>2</sub> and H <sub>2</sub> O molar fractions at a cell voltage of 0.5 V for three different temperatures..	103
Figure 6.5: O <sub>2</sub> molar fractions at a cell voltage of 0.5 V for three different temperatures .....	104
Figure 6.6: local current density profile along the anode thickness for humidified H <sub>2</sub> at 700°C. ....	104
Figure 6.7: Experimental (dotted lines) and simulated (solid lines) cell performance using 20%CO/80%CO <sub>2</sub> at 700, 650 and 600°C.....	105
Figure 6.8: CO and CO <sub>2</sub> molar fractions at 700°C for two different cell voltages (0.7 and 0.5V) and a feed gas composition of 20%CO/80%CO <sub>2</sub> .....	106
Figure 6.9: O <sub>2</sub> molar fraction at 700°C for two different cell voltages (0.7 and 0.5V) and a feed gas composition of 20%CO/80%CO <sub>2</sub> .....	107



Figure 6.10: CO and CO <sub>2</sub> molar fractions at a cell voltage of 0.5V for three different temperatures and for a feed gas composition of 20%CO/80%CO <sub>2</sub> .....	108
Figure 6.11: O <sub>2</sub> molar fractions at a cell voltage of 0.5V for three different temperatures and for a feed gas composition of 20%CO/80%CO <sub>2</sub> .....	108
Figure 6.12: Polarization curve for 20%H <sub>2</sub> /80%H <sub>2</sub> O (shown as “H <sub>2</sub> ” in the figure legend) and for 20%CO/80%CO <sub>2</sub> (shown as “CO” in the figure legend) .....	109
Figure 6.13: Experimental (dotted lines) and simulated (solid lines) cell performance for syngas from diesel, pre-reformed natural gas and biomass gasification at 700°C.....	111
Figure 6.14: Simulation results without WGS on SDC (dotted lines) and with WGS on SDC (solid lines) at 700°C .....	112
Figure 6.15: H <sub>2</sub> mole fraction without WGS on SDC (solid lines) and with WGS on SDC (dotted lines) incorporation at 700°C and at two different cell voltages (0.7V and 0.4V). a) biomass syngas, b) diesel syngas, c) pre-reformed natural gas .....	114
Figure 6.16: CO mole fraction without WGS on SDC (solid lines) and with WGS on SDC (dotted lines) incorporation at two different cell voltages (0.7V and 0.4V). a) biomass syngas, b) diesel syngas, c) pre-reformed natural gas.....	115
Figure 6.17: Reaction quotient without WGS on SDC (solid lines) and with WGS on SDC (dotted lines) at 700°C and for two different cell voltages (0.7V and 0.4V). a) biomass syngas, b) diesel syngas, c) pre-reformed natural gas.....	117
Figure 6.18: Reaction rate of WGS on SDC (solid lines) and reaction rate of WGS on Ni (dotted lines) at 700°C and at two different cell voltages (0.7V and 0.4V). a) biomass syngas, b) diesel syngas, c) pre-reformed natural gas.....	119



## List of Tables

Table 2.1: Types of fuel cells (Li, 2006; O'Hayre et al., 2006) .....	7
Table 2.2: Anodic and cathodic reactions of fuel cells (Selman and Lin, 1993) .....	8
Table 2.3: Summary of various key SOFC model developments .....	31
Table 3.1: Methane steam reforming evaluation parameters .....	41
Table 4.1: Ratio of CO <sub>2</sub> conversion over SDC to YSZ.....	57
Table 4.2: Kinetic study experimental data .....	61
Table 4.3: Reverse water-gas shift rate expressions depending on the rate limiting step based on Liu et al. (2010) mechanism.....	68
Table 4.4: Kinetic parameters of reverse WGS reaction when the surface reaction I is rate limiting .	72
Table 4.5: Reverse WGS activation energy from literature .....	76
Table 4.6: The parameters estimates and standard deviation obtained from MCMC analysis using all four temperatures with Tref= 998 K .....	82
Table 4.7: The parameters estimates and standard deviation obtained from MCMC analysis at 998 K .....	84
Table 5.1: Constant for the semi-empirical form of $\Delta Gr_{xn}, To$ .....	88
Table 5.2: Values for $\sigma_i$ and $\epsilon_i/k$ parameters for gases of interest in this work (Reid et al., 1987) .....	91
Table 5.3: Gas Diffusion Volume (m <sup>3</sup> /mol).....	92
Table 5.4: List of boundary conditions for mass-transport.....	95
Table 5.5: List of boundary conditions for the ionic transport equations .....	97
Table 5.6: List of boundary conditions for the electronic transport equations .....	97
Table 6.1: Simulation parameter at 700°C.....	99
Table 6.2: Species composition of syngas .....	110

## Nomenclature

### List of English symbols

$D_{ij}$	Binary diffusion coefficient
$D_{ik}^{eff}$	Effective Knudsen diffusion coefficients
$D_{im}^{eff}$	Effective molecular diffusion coefficient
$\mathbf{d}_k$	Diffusional driving force acting on species $k$
$E_a$	Activation energy
$E_{a,e}$	Activation energy for the electronic conductivity
$E_{a,i}$	Activation energy for the ionic conductivity
$E_{cell}$	Cell potential
$E^o$	Reversible fuel cell voltage
$F$	Faraday's constant
$F_i$	Molar flow rate of species $i$
$F_I$	Flow rate of inert
$F_T$	Total flow rate
$i_o$	Exchange current density
$J$	Current density
$k$	Reaction rate constant
$K$	Equilibrium constant
$M$	Molecular weight
$N_i$	Molar flux of species $i$
$n_i^{in}$	Inlet molar flow rate of species $i$
$n_i^{out}$	Outlet molar flow rate of species $i$
$P$	Pressure
$r$	Reaction rate
$R$	Gas constant
$T$	Temperature
$V$	Voltage

$v_i$	Molar diffusion volume of species $i$
$V_{\text{ref}}$	Relative potential difference between the electronic and ionic conductors
$W$	Mass of catalyst
$X_i$	Conversion of species $i$
$Y_i$	Product yield of species $i$
$\Delta G_i$	Standard Gibb's energy of species $i$
$\dot{S}_c$	Rate of production or consumption of electric charge

### **List of Greek symbols**

$\eta_{\text{ohm}}$	Ohmic overpotential
$\eta_{\text{act}}$	Activation overpotential
$\eta_{\text{con}}$	Concentration overpotential
$\eta_T$	Total overpotential
$\alpha$	Exchange transfer coefficient
$\varepsilon_{ij}$	Characteristic Lennard-Jones energy
$\rho$	density in $\text{kg/m}^3$
$\sigma$	Conductivity
$\sigma_{E,i}$	Standard electronic conductivity
$\sigma_i$	Diameter of the molecular collision
$\sigma_{o,i}$	Standard ionic conductivity
$\tau$	Tortuosity factor for molecular diffusion
$\varphi$	Porosity of the porous structure
$\Omega_D$	Collision integral
$\omega_i$	Mass fraction of species $i$

### **List of abbreviations and acronyms**

AFC	Alkaline Fuel Cell
CHP	combined heat and power



GHSV	Gas Hourly Space Velocity
IT-SOFC	Intermediate Temperature Solid Oxide Fuel Cell
JCRs	Joint Confidence Regions
LSM	Strontium doped Lanthanum Manganite
MCFC	Molten Carbonate Fuel Cell
MCMC	Markov Chain Monte Carlo
MFCs	Mass-Flow Controllers
MSR	Methane Steam Reforming
Ni-SDC	Nickel-Samaria Doped Ceria
OCV	Open Circuit Voltage
PAFC	Phosphoric Acid Fuel Cell
PEMFC	Polymer Electrolyte Membrane Fuel Cell
RWGS	Reverse Water Gas Shift RWGS
SDC	Samaria-Doped Ceria
SOFC	Solid Oxide Fuel Cell
TPB	Three Phase boundary
WGS	Water Gas Shift
YSZ	Yttria-Stabilized Zirconia

# Chapter 1

## Introduction

One of the major drivers to accelerate the development of fuel cells is the increasing concern about the environmental consequences of the continuous use of fossil fuels for both stationary and transportation applications. With the rising concern about greenhouse gas emissions, many efforts are being pursued to develop more efficient energy conversion devices to replace conventional combustion heat engines. Fuel cell technologies offer efficient and clean conversion of chemical energy of fuels to electrical energy. The waste stream from a fuel cell using  $H_2$  fuel contains primarily water and heat, thereby greatly reducing greenhouse gases. Even for the fuel cells that can operate on hydrocarbons, the greenhouse gas emissions can be significantly reduced due to the higher efficiency. Also, the operation of some fuel cells (e.g. solid oxide fuel cell, SOFC) are such that  $CO_2$  capture could potentially be implemented with relatively low penalty since the cell exhaust is composed mainly of  $CO_2$  and water. Therefore, research focusing on the improvement of performance of SOFCs is increasing.

In addition, since no nitrogen oxides or particulates are emitted, fuel cells are known as a very clean technology. With rising fuel prices and stricter emission control regulations, these capabilities make fuel cells even more attractive.

Solid Oxide Fuel Cell (SOFC) is a type of high temperature fuel cell which operates at about  $1000^\circ C$  and is thus capable of producing both electricity and heat. A very important advantage of SOFC is that it can tolerate many types of fuel, including hydrocarbon fuels, natural gas, synthesis gas (syngas) and humidified hydrogen ( $H_2$ ) (Shi and Cai, 2006). Furthermore, since SOFC operates at high temperatures, SOFC can reform hydrocarbon fuels internally. Internal reforming in a SOFC simplifies the overall system design because the external reformer can be eliminated. A SOFC system with internal reforming has an inherent advantage in terms of energy efficiency because the heat required for the reforming reaction is supplied by the heat generated by the electrochemical reaction. Moreover, the ceramic

thickness of the electrodes, and not only at the boundary between the electrode and electrolyte.

### **1.1 Motivation of the Research**

Recently, many efforts have been made toward developing intermediate-temperature SOFC (IT-SOFC) operating in the temperature range 600-800°C, because such temperatures enable the use of low cost metallic interconnects, shorter start-up time and improved long-term stability of cell materials by reducing the material degradation rate. Unfortunately, decreasing the operating temperature increases the ohmic overpotential due to higher ionic diffusion in the electrolyte resistance, thereby reducing electrochemical performance. To alleviate this problem, designs of IT-SOFC aim at reducing the thickness of the electrolyte while increasing that of the anode. In such design, ohmic losses are reduced. Therefore this research focused on anode supported cell which is done via a combination of mathematical modelling and experimental validation. Methane reforming reaction and water-gas shift reaction have been taken into account in the modelling for syngas composition. For the water gas shift reaction, it was assumed that this reaction occurs not only on Ni (like all reported studies assumed), but also on SDC. The electrochemical reactions were assumed to be able to occur along the thickness of the electrodes, and not only at the boundary between the electrode and electrolyte.

There are two specific objectives in this work:

- 1) Determine the reaction rate expression for water gas shift reaction on SDC.
- 2) Develop a 1D model that can predict the performance of the cell and on the Ni/SDC material under different operating conditions (e.g. temperature, current density, fuel composition).

In order to achieve these objectives, two research scopes have been considered:

- 1) Kinetic Study: Developed a kinetic expression for the reverse water gas shift reaction combining experiments and calculations using Matlab codes involving a non-linear least square problem (lsqcurvefit command).



- 2) Modelling Study: Developed a one-dimensional mechanistic model of anode supported button cells that considers that electrochemical reaction occurs not only at anode/electrolyte interface to predict SOFC performance. The model was validated with experimental data produced in the SOFC group at the University of Waterloo.

## **1.2 Research Contributions**

- 1) Developed the first Ni/SDC model validated for various fuel compositions; 97% $\text{H}_2$ /3% $\text{H}_2\text{O}$ , 20% $\text{CO}$ /80% $\text{CO}_2$ , syngas compositions (diesel, biomass, pre-reformed natural gas). At the time of writing this thesis, there is only one paper in the literature (Cui et al., 2010) dealing with SDC-electrolyte SOFC modeling, but their model was validated only with humidified hydrogen.
- 2) Demonstrated that SDC is active towards the water gas shift reaction (WGS) and determined the kinetic parameters of WGS using Matlab codes involving solving a non-linear least square problem (lsqcurvefit command). The WGS on SDC was then incorporated in the modeling study.

## **1.3 Thesis Outline**

This thesis is organised into seven chapters, as follows:

Chapter 1 presents an introduction of the research and discusses the motivation of the research, its objectives and its contribution.

Chapter 2 presents a general discussion about fuel cells and an overview of several studies on SOFC single cell modelling.

Chapter 3 describes the experimental techniques including material preparation to study the activity of methane steam reforming (MSR) and kinetics of water gas shift reaction.

Chapter 4 demonstrates the activity of SDC toward the water-gas shift reaction and describes the kinetic study of the water gas shift reaction on SDC.

Chapter 5 describes the model formulation for a 1D SOFC model of button cell.

Chapter 6 discusses the results of the modelling study involving  $\text{H}_2/\text{H}_2\text{O}$ ,  $\text{CO}/\text{CO}_2$  and syngas compositions.

Chapter 7 presents the conclusions and recommendations for this work.

## **Chapter 2**

### **Literature Review**

#### **2.1 Introduction**

This chapter begins with a general discussion about fuel cells, and then focuses on solid oxide fuel cells (SOFC) including SOFC fuels, materials, cell design and performance. In the last section (section 2.4), an overview of several studies on SOFC modelling is provided.

#### **2.2 Fuel Cells in Brief**

The fuel cell, an electrochemical energy conversion device which directly converts chemical to electrical energy, is a promising technology for producing electricity cleanly and efficiently. The invention of fuel cells as energy conversion systems began in the middle of the 19th century (Hirschenhofer et al., 1998; Stambouli and Traversa, 2002). Because of its high energy efficiency and being environmentally friendly, fuel cells are considered to be potentially attractive devices to produce electricity.

Fuel cells exist in different types. There are five major types of fuel cells: phosphoric acid fuel cell (PAFC), polymer electrolyte membrane fuel cell (PEMFC), alkaline fuel cell (AFC), molten carbonate fuel cell (MCFC) and solid oxide fuel cell (SOFC). The types of fuel cells differ primarily by the type of electrolyte they employ, charge carrier, operating temperature, material, fuel tolerance and performance characteristics, as listed in Table 2.1.

Although the five types of fuel cells have different characteristics, the basic structure of all fuel cells is similar. The cell consists of two electrodes called anode and cathode separated by an electrolyte and connected to an external circuit. A schematic representation of a fuel cell with the reactant and product and the ion conduction flow directions through the cell is shown in Figure 2.1.



**Table 2.1: Types of fuel cells (Li, 2006; O'Hayre et al., 2006)**

Characteristic	Type of fuel cells				
	PEMFC	PAFC	AFC	MCFC	SOFC
Electrolyte	Polymer membrane	Liquid $\text{H}_3\text{PO}_4$ (immobilized)	Liquid KOH (immobilized)	Molten carbonate	Ceramic
Charge carrier	$\text{H}^+$	$\text{H}^+$	$\text{OH}^-$	$\text{CO}_3^{2-}$	$\text{O}^{2-}$
Operating temperature ( $^{\circ}\text{C}$ )	50-80	160-220	60-220	600-700	600-1000
Catalyst	Platinum (cathode / anode)	Platinum (cathode / anode)	Platinum (cathode / anode)	Nickel (cathode / anode)	Ni: anode $\text{LaSrMnO}_3$ : cathode
Cell component	Carbon based	Carbon based	Carbon based	Stainless based	Ceramic based
Fuel compatibility	$\text{H}_2$ , methanol	$\text{H}_2$	$\text{H}_2$	$\text{H}_2$ , $\text{CH}_4$	$\text{H}_2$ , $\text{CH}_4$ , $\text{CO}$
Fuel efficiency (Chemical to electrical)	45-60	55	40-60	60-65	55-65

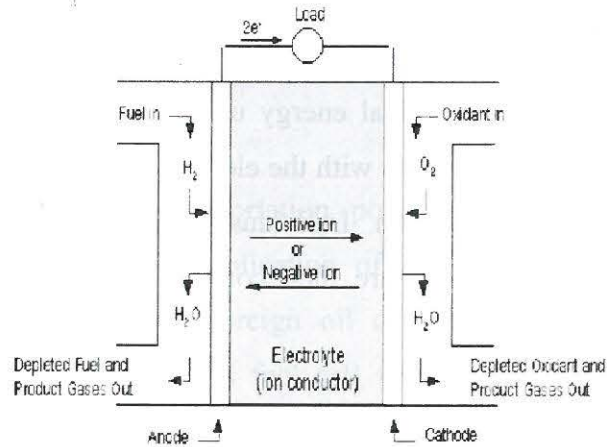


**Figure 2.1: Diagram of a single fuel cell (Lisbona et al., 2005)**

In a typical fuel cell, gaseous fuels (e.g. hydrogen) are fed continuously to the anode and an oxidant (typically oxygen from air) is fed continuously to the cathode. The electrochemical reactions take place in the electrodes to produce an electric current. The function of the electrolyte is to conduct ionic charges between the electrodes (Lisbona et al., 2005). Individual fuel cells have a maximum output voltage on the order of 1 V. Substantial

voltages and power outputs are obtained by connecting many cells electrically in series to form a fuel cell stack.

All five fuel cell types have different electrochemical reactions. The electrochemical reactions occurring at the anode and cathode sides are summarized in Table 2.2.

**Table 2.2: Anodic and cathodic reactions of fuel cells (Selman and Lin, 1993)**

Fuel Cell	Anode Reaction	Cathode Reaction
PEMFC	$\text{H}_2 \rightarrow 2\text{H}^+ + 2\text{e}^-$	$\text{O}_2 + 4\text{H}^+ + 4\text{e}^- \rightarrow 2\text{H}_2\text{O}$
PAFC	$\text{H}_2 \rightarrow 2\text{H}^+ + 2\text{e}^-$	$\text{O}_2 + 4\text{H}^+ + 4\text{e}^- \rightarrow 2\text{H}_2\text{O}$
AFC	$\text{H}_2 + 2\text{OH}^- \rightarrow 2\text{H}_2\text{O} + 2\text{e}^-$	$\text{O}_2 + 2\text{H}_2\text{O} + 4\text{e}^- \rightarrow 4\text{OH}^-$
MCFC	$\text{H}_2 + \text{CO}_3^{2-} \rightarrow \text{H}_2\text{O} + \text{CO}_2 + 2\text{e}^-$ $\text{CO} + \text{CO}_3^{2-} \rightarrow 2\text{CO}_2 + 2\text{e}^-$	$\text{O}_2 + 2\text{CO}_2 + 4\text{e}^- \rightarrow 2\text{CO}_3^{2-}$
SOFC	$\text{H}_2 + \text{O}^{2-} \rightarrow \text{H}_2\text{O} + 2\text{e}^-$ $\text{CO} + \text{O}^{2-} \rightarrow \text{CO}_2 + 2\text{e}^-$	$\text{O}_2 + 4\text{e}^- \rightarrow 2\text{O}^{2-}$

The operational principles of fuel cells and batteries have similarities: both are galvanic cells. They consist of an anode and a cathode in contact with an electrolyte. Both devices generate electrical energy by converting chemical energy using an electrochemical reaction. These reactions occur at the anode and cathode with the electron transfer forced through an external load in order to complete the reaction. Individual cells of both batteries and fuel cells generate only small voltages, which are then combined in series to achieve substantial voltage and power capacities.

Fuel cells differ from batteries in which the chemical reactants are stored. In a battery, the anode and cathode are consumed during use. Thus, a battery can only operate until these materials are fully consumed after which it either must be replaced or recharged, depending on the nature of the materials. In a fuel cell, the chemical reactants are supplied from an external source so that its materials of construction are never consumed and do not need to be recharged. A fuel cell continues to operate as long as reactants are supplied and the reaction products are removed (O'Hayre et al., 2006).

The choice of electrochemical device, either battery or fuel cell, depends upon use. For larger scale applications, fuel cells have several advantages over batteries including smaller size, lighter weight, quick refuelling and longer range.

Fuel cells and combustion engines also share some similarities. Both fuel cells and internal combustion engines completely oxidize the fuel. Fuel cells use pure hydrogen or a reformat gas mixture. Internal combustion engines typically use hydrogen containing fossil fuels directly, although they could be configured to operate using pure hydrogen. Both systems use air as the oxidant. In some respects, fuel cells and internal combustion engines are fundamentally different. Fuel cells react the fuel and oxidant electrochemically whereas internal combustion engines react the fuel and oxidant through combustion. Like other electrochemical devices, fuel cells are not limited by the Carnot efficiency as combustion engines are (Lisbona et al., 2005). For example, when ethanol is burned in a combustion engine, the energy efficiency is limited by the Carnot efficiency and can reach, in practice, only about 25%. This fuel efficiency can be significantly increased when ethanol is first converted to hydrogen and then used in a fuel cell with an efficiency of more than 50% (Rass-Hansen et al., 2007).

Applications of fuel cells are in transportation, power generation and in powering mobile devices (Shi and Cai, 2006). The application of fuel cells in the transportation sector increases fuel efficiency, decreases foreign oil dependency and becomes an important technology to fight climate change. As fuel cell vehicles begin to operate on fuels from natural gas or gasoline, greenhouse gas emissions will be reduced. The PEM fuel cell is regarded as ideally suited for transportation applications due to its high power density, high energy conversion efficiency, compactness, lightweight nature and low operating temperature (below 100°C).

For stationary power generation applications, both low-temperature and high-temperature fuel cells could be utilized. The low-temperature fuel cells have the advantage that usually a



faster start-up time can be achieved, which makes it more attractive for small-power generation. The high-temperature systems such as SOFC and MCFC generate high-grade heat which can be used directly in a heat cycle or indirectly by incorporating the fuel cell system into a combined cycle. SOFC and MCFC are more suitable for large-scale power plants (Dokiya, 2002). SOFCs are expected to play a significant role in residential combined heat and power (CHP) applications (1 to 10 kW) and commercial CHP applications (up to 250 kW), or power plant stationary applications (Wei Zhang, 2006).

### **2.3 Solid Oxide Fuel Cell**

SOFC is a high temperature fuel cell operating around 1000°C for state-of-the-art SOFCs, composed of a YSZ (Yttria-Stabilized Zirconia,  $(Y_2O_3)_{0.08} (ZrO_2)_{0.92}$ ) electrolyte, Ni-YSZ anode, LSM (Strontium doped Lanthanum Manganite,  $La_{1-x}Sr_xMnO_3$ ) and cathode (Singhal, 2000; Zhu and Deevi, 2003). An advantage of the high operating temperature is the possibility of combined heat and power generation which would even further increase the efficiency of this technology (Singhal, 2000). An even more important advantage of SOFC compared to low temperature fuel cells (e.g. PEMFC) is not only the lower cost of the electrocatalyst (Ni for SOFC, as opposed to Pt for PEMFC), but also that they are tolerant to CO, making SOFC fuel flexible (Stambouli and Traversa, 2002). Moreover, the high operating temperature allows internal reforming of the fuel to form  $H_2$  and CO, where the heat released by the electrochemical reaction can be utilized by the endothermic steam reforming reaction (Ahmed and Foger, 2000). Internal reforming can also lower the overall system costs because steam required for the steam reforming can be obtained from the steam generated by the electrochemical fuel cell reaction, and because of reduced maintenance due to the elimination of an external reformer (Clarke et al., 1997; Boder and Dittmeyer, 2006; Cheekatamarla et al., 2008). All of these advantages make the SOFC an even more attractive means for producing electrical power.



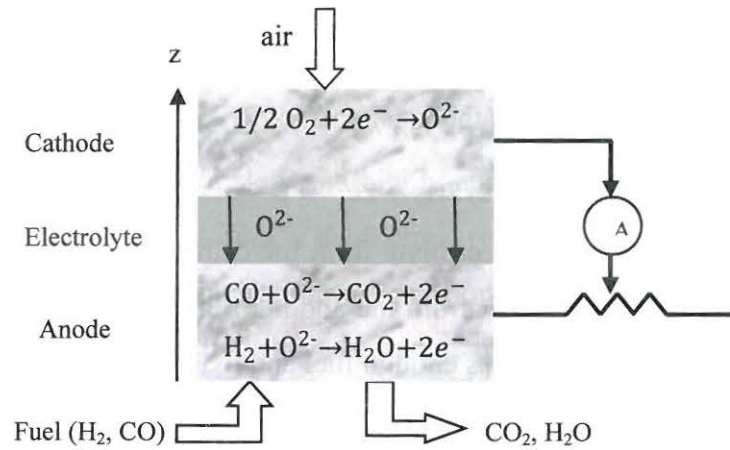


**Figure 2.2: Schematic diagram of SOFC operation**

Figure 2.2 shows the main components of a SOFC, consisting of two electrodes, called anode and cathode, separated by a dense solid electrolyte. The electrodes are porous to facilitate the transport of fuel and oxidant from the gas channels to the three phase boundaries where electrochemical reactions occur. Within an SOFC anode structure, the hydrocarbon's fuel may be reformed via heterogeneous reaction to produce  $\text{H}_2$  and  $\text{CO}$  in the presence of a reforming catalyst (e.g.  $\text{Ni}$ ). The  $\text{CO}$  may further react with  $\text{H}_2\text{O}$  to form  $\text{H}_2$  and  $\text{CO}_2$  via the water-gas-shift reaction. Within the anode, the pore spaces are typically sufficiently small that the most likely collisions are between gas molecules and surfaces, and there is very little probability for gas-gas collisions. Consequently, gas phase homogeneous kinetics are usually negligible (Hecht et al., 2005; Zhu and Kee, 2008).

The electrolyte is dense to keep the gases separated and to allow an oxygen concentration difference between the anode and the cathode. Oxygen ions are produced at the three phase boundaries near the cathode/electrolyte interface and are transported by a solid-state migration mechanism through the electrolyte to the anode/electrolyte interface, where oxygen ions react with the fuel (Badwal, and Foger, 1996). Products generated from the reaction are transported back to the fuel channel through pores.

The electrochemical reactions at the anode are:



The electrochemical reaction at the cathode is:



The  $\text{O}^{2-}$  ion is drawn through the electrolyte from the cathode to the anode, while electrons are forced through an external circuit from the anode to the cathode. These electrochemical reactions occur continuously as long as enough fuel and oxidant are supplied to the SOFC.

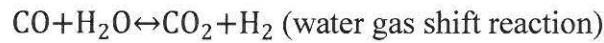
#### SOFC Fuel:

As was previously stated, one of the major advantages of SOFC is fuel flexibility: fuels that can be used in a SOFC can be hydrogen ( $\text{H}_2$ ), carbon monoxide ( $\text{CO}$ ), methane ( $\text{CH}_4$ ) or some higher hydrocarbons and synthesis gas from solid fuels (coal and biomass) (Li et al., 2010). This feature reduces considerably the cost intensive efforts for producing high quality pure hydrogen, as demanded by other types of low temperature fuel cells.

Hydrocarbon based fuels, such as methane, can be reformed to produce  $\text{H}_2$  and  $\text{CO}$ . Reforming is a chemical process that reacts hydrogen-containing fuels in the presence of steam, oxygen, or both, into a hydrogen-rich gas stream. The resulting hydrogen-rich gas mixture is called reformat. Reforming can be further subdivided according to whether (1) it occurs in a chemical reactor outside the fuel cell (external reforming) or (2) it occurs at the catalyst surface inside the fuel cell itself (internal reforming), the latter being possible in high temperature fuel cells.

Methane steam reforming is one of the most widely used processes for the production of  $\text{H}_2$  and  $\text{CO}$  mixtures. In fact, methane steam reforming accounts for 95% of the hydrogen produced in the United States (Blaylock et al., 2009). Methane steam reforming is an endothermic reaction and is normally carried out at temperatures around 700-800°C in the presence of a suitable catalyst. Nickel used as anode material can act as a methane steam

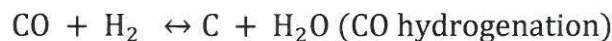
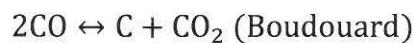
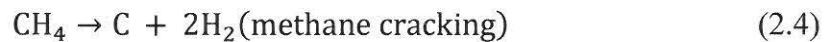
reforming catalyst. In the reforming of the methane with steam, the dominant reactions are the following two reactions:



The steam reforming reaction is a slow and highly endothermic reaction, and the water gas shift (WGS) reaction is a fast and weakly exothermic reaction. Therefore, the overall reaction resulting from the methane steam reforming reaction and the water gas shift reaction is highly endothermic. Several authors have assumed that the water gas shift reaction is at equilibrium at the reforming temperature (Nagata et al., 2001).

Methane steam reforming is affected by operating pressure, temperature and the ratio of steam to carbon in the feed gas. Methane steam reforming is favourable at low pressure, high temperature and high steam-to-carbon ratio.

Although internal reforming offers an advantage in terms of reducing the overall system cost, it also poses the problem of carbon deposition with the use of Ni-based catalyst which deteriorates the performance of the cell. Methane tends to dissociate on the surface of the nickel particles, depositing carbon, and the CO produced through MSR can also contribute to carbon deposition, as indicated by the following reactions:



The formation of carbon is a serious problem in solid oxide fuel cells fed with hydrocarbons. Although the ability to utilize hydrocarbons as a fuel is an important attribute of SOFC, because of carbon formation problems associated with pure hydrocarbon fuels, practical SOFC systems usually operate with mixtures of H<sub>2</sub>, CO, and hydrocarbons (Hecht et al., 2005). In addition to reducing carbon formation, mixing the hydrocarbon fuel with H<sub>2</sub> and CO can also avoid thermal stresses in the SOFC, as regions where the highly endothermic